Dynamic Multi-Coil Shimming of the Human Brain at 7 Tesla

Christoph Juchem[1], **Terence W. Nixon**[1], **Scott McIntyre**[1], **Vincent O. Boer**[2], **Douglas L. Rothman**[1], and **Robin A. de Graaf**[1]

[1]Yale University School of Medicine, Department of Diagnostic Radiology, MR Research Center (MRRC), 300 Cedar Street, New Haven, CT 06520, USA [2]UMC Utrecht, Department of Radiology, Utrecht University, Utrecht, The Netherlands

Abstract

High quality magnetic field homogenization of the human brain (i.e. shimming) for MR imaging and spectroscopy is a demanding task. The susceptibility differences between air and tissue are a longstanding problem as they induce complex field distortions in the prefrontal cortex and the temporal lobes. To date, the theoretical gains of high field MR have only been realized partially in the human brain due to limited magnetic field homogeneity.

A novel shimming technique for the human brain is presented that is based on the combination of non-orthogonal basis fields from 48 individual, circular coils. Custom-built amplifier electronics enabled the dynamic application of the multi-coil shim fields in a slice-specific fashion. Dynamic multi-coil (DMC) shimming is shown to eliminate most of the magnetic field inhomogeneity apparent in the human brain at 7 Tesla and provided improved performance compared to state-of-the-art dynamic shim updating with zero through third order spherical harmonic functions. The novel technique paves the way for high field MR applications of the human brain for which excellent magnetic field homogeneity is a prerequisite.

Keywords

magnetic field modeling; multi-coil; whole brain; shimming; spherical harmonic functions; dynamic shim updating

INTRODUCTION

Magnetic field homogeneity is an essential prerequisite for most MR imaging and spectroscopy applications to guarantee the correct spatial registration, the best signal strength and optimal spectral resolution [1; 2]. Varying magnetic susceptibility conditions around the human brain, however, cause strong and complex magnetic field distortions inside the brain [3; 4] and reduce the informative value of the results. The ongoing trend in the MR community towards scanners with higher B_0 fields for increased signal strength, spectral dispersion and BOLD sensitivity [5] further magnifies the problem as the induced

Address correspondence to: Christoph Juchem, MR Research Center (MRRC), 300 Cedar Street, TAC N142, New Haven, CT 06520, USA, Phone: +1 (203) 785-7021, Fax: +1 (203) 785-6643, christoph.juchem@yale.edu.

magnetic field distortions scale linearly with the scanner B_0 field strength. Particularly strong and localized magnetic field artifacts are observed in the prefrontal cortex (PFC) and the temporal lobes (TLs). The PFC is involved in working memory and cognitive control [6; 7] and dysfunction manifests itself in neuropsychiatric illnesses such as bipolar disorder, schizophrenia, or post-traumatic stress disorder [8]. Similarly, the TLs are of prime interest due to their role in high-level visual processing [9] and their relevance for pathologies like temporal lobe epilepsy [10]. A deeper understanding of the individual significances of these brain areas as well as their functional connectivity with other parts of the brain can be gained with functional MR imaging or through the quantification of neurochemicals with MR spectroscopy [5]. Other lines of research addressing e.g. the brains' resting state connectivity with functional MR imaging [11] or the diagnosis of brain trauma and neurodegenerative diseases with susceptibility weighted imaging [12] are typically not focused on selected brain regions. Instead, the entire brain is considered with these methods from its dorsal end to the ventral brain structures such as the thalamic nuclei, the cerebellum or the medulla oblongata [11; 12]. The obtained quality of all of these imaging and spectroscopy methods remains limited by the achievable magnetic field homogeneity. To date, the theoretical gains of various high field MR applications have only been realized partially in the human brain due to limited magnetic field homogeneity in larger volumes such as brain slices or the brain as a whole [13].

The most commonly employed method for magnetic field homogenization of the human brain decomposes the apparent magnetic field distribution in to a set of spherical harmonic (SH) basis functions. The corresponding correction (i.e. shim) fields are then generated by a scaled superposition of the contributing basis fields, with each SH term generated by a dedicated coil. The experimentally available low order SH terms are capable of resembling and, therefore, shimming large-scale and shallow magnetic field components. However, the complexity of the magnetic field distortions encountered in the human brain is beyond their shaping capability [3]. This is especially true for the artifacts that are generated by the sinuses in the PFC and by the auditory cavities in the TLs which cannot be corrected adequately as much higher orders would be necessary to fully compensate them.

In reality, due to the lack of satisfactory whole brain SH shimming, the shim procedures as well as the subsequent MR experiments are often limited to single brain slices [14; 15] or cubic volumes [16] to better exploit the capabilities of the SH functions. Successful methods have been presented to provide efficient and reliable magnetic field optimization in these selected geometries [14–16]. Dynamic spherical harmonics (DSH) shimming employs this principle for the homogenization of larger volumes by breaking them down into subvolumes such as single slices or voxels that are compatible with the MR experiment [4; 17–20]. The fast adjustment of volume-specific shim settings then allows the optimization of the magnetic field homogeneity over the entire brain based on the improvement in the constituent subvolumes within the same experiment. While significant improvements in magnetic field homogeneity have been demonstrated for most parts of the human brain, even zero through third order DSH shimming is not capable of completely homogenizing the entire human brain [4].

Various attempts have been made to specifically address the magnetic field distortions in the most problematic areas of the human brain with dedicated passive [21; 22] and active [23] shimming methods. While each approach has merits, most strategies have significant limitations such as limited field accuracy, limited flexibility to account for inter-subject variation or because they artificially affect other brain areas. The specific tailoring of a set of localized electrical coils to the artifact in the human PFC allowed, together with conventional SH field terms, the removal of large parts of the encountered magnetic field inhomogeneity without affecting the rest of the brain [3].

It has been demonstrated recently that a set of generic, circular coils can be converted to a powerful magnetic field modeling system when each of the electrical coils is driven individually [24]. The flexible and accurate synthesis of simple and complex magnetic field shapes has been enabled by a repertoire of non-orthogonal basis fields that provide localized gradient patterns close to the coils and shallow component farther away. After the introduction of the multi-coil (MC) concept for the synthesis of low order SH fields, static and especially dynamic MC (DMC) shimming has been shown to outperform conventional, low order SH shimming in the mouse brain [25].

The current publication builds upon previous work by translating the DMC shimming concept from the rodent to the human brain. DMC shimming is demonstrated to be capable of modeling and removing large parts of the magnetic field inhomogeneity encountered in the human brain at 7 Tesla and to exceed the performance of earlier shimming methods based on SH functions, including zero through third order DSH shimming.

METHODS

General Experimental Setup

The study involved MR field mapping and shim experiments on six healthy volunteers (three women, three men, age 26–39 years) in accordance with Institutional Review Board guidelines for research on human subjects. Experiments were performed on an Agilent 7 Tesla magnet with a 68 cm bore diameter interfaced to a DirectDrive spectrometer operating at 298.1 MHz for protons. The system was equipped with custom-designed, actively-shielded gradients (42 cm inner diameter, 50 mT/m in 512 µs, Magnex Scientific, Oxford, UK) and operated with VnmrJ 2.3A software (Agilent, Santa Clara, CA). An 8-element RF array coil with an inner diameter of 25 cm was used for RF transmission and reception [26]. Shimming of the transmit field B_1^+ was achieved through in-house developed MR methods and software with B_1^+ mapping based on Bloch-Siegert shifts [27]. A custom-made B_0 field mapping sequence with multiple echo times (delays 0/0.2/0.5/1.5/3.0 ms, field-of-view $210 \times 210 \times 120$ mm^3, matrix $70 \times 70 \times 40$) was used to measure magnetic field distributions in the unshimmed brain and with experimental DMC shimming. Phase maps were calculated through voxel-by-voxel temporal phase unwrapping and B_0 field maps were computed using linear regression of signal phase and echo time [1] in combination with an echo-time exclusion algorithm for the minimization of frequency noise [24]. The brain selection necessary for the shim analysis was achieved by a combination of criteria including signal-to-noise thresholding, magnetic field error analysis and voxel clustering [4; 25].

Design and Implementation of Dynamic Multi-Coil Shimming of the Human Brain

The main focus of the current study was to demonstrate the performance of the MC matrices for shimming the entire human brain at 7 Tesla. As such the employed head volume coil, consisting of an 8-channel Tx/Rx array, was chosen as a starting point for the MC matrix construction and no efforts were made for the mutual optimization of the RF and the MC setups. Given the geometrical restrictions of the RF coil, the DMC setup was designed to be on the inside of the RF array. To this end, a matrix of 48 circular, constant-current coils was derived on an elliptical cylinder shape (Fig. 1A). The coils were arranged in 4 rows of 12 coils to closely surround the brain of the human subjects and to provide a large repertoire of magnetic field shapes given the available space between the head of the subjects and the cover of the RF coil. For simplicity, all coils used the same diameter (center diameter 47 mm) which was determined from the total circumference of the former of 68 cm divided by the 12 coils per MC ring while considering the extension of realistic coil bundles and the space requirements for their mounting. Based on experiences from previous coil setups [3], 100 turns per coil were chosen as a trade-off between space requirements, provided field

amplitudes and concomitant heat generation. Note that adjacent MC rows were rotated by half a coil diameter with respect to each other to allow a closer packing. Previous studies on mouse brain [24] have demonstrated a damping of the RF field when the MC array is placed between the RF coil and the subject. In order to minimize distortions of the RF field in the current human design, a central 10 cm band was chosen to remain uncovered by MC coils to minimize interactions with the 8-cm long RF array elements (Fig. 1C). Besides the positioning of the MC rings, this was achieved by flattening the coils of the inner two MC rings towards the RF array. A similar flattening on the outside of the outer two MC rings was applied to limit the overall longitudinal extension of the MC setup and to prevent conflicting space requirements with the subjects' shoulders. In addition, some parts of the two coils closest to the nose opening of the MC former were removed to prevent any contact between the shim coils and the subject. During the design process, magnetic field simulations based on the Biot-Savart law were used to predict and optimize the DMC shim performance as a function of the details of the coil matrix given the available set of 48 individual current amplifiers. Note that the resultant MC setup does not necessarily represent the optimal solution as some practical decisions had to be made to account for the space requirements of the subjects' head in combination with the geometric constraints of the RF coil.

In its experimental realization, the coils were made of heavy armored polythermaleze copper wire (Belden Electronic Division, St. Louis/MO, USA) of 0.4 mm diameter leading to an effective coil thickness of approximately 5 mm. The 48 coils were mounted on the outside of an acrylic former with outer diameters of 20 and 23 cm (Fig. 1B). In-house developed and built constant-current amplifier electronics [28] allowed well-defined current alterations in the individual coils (680 µH) over the full dynamic range of ±1 A in 200 µs. Software written in C and executed on the Agilent console computer was used to control the MC shim interface via the serial port with the RS232 protocol. Each MC channel was calibrated based on 7 independent 3-dimensional field mapping experiments that covered the dynamic range of the corresponding current power supply as described in [24]. For DMC shimming, slice-specific sets of MC currents were loaded to local memory of the MC shim interface and applied under the control of the pulse program in a slice-specific fashion via real-time TTL pulses from the scanner [28]. In order to minimize heat-related hazardous risks to the subjects and the hardware, eight-channel real-time temperature monitoring with T-type thermocouples (Omega Engineering, Stamford, CT) was present at all times. The temperature measurements focused on coils with typically high current requirements (as determined from simulations), coils with little space between the MC former and the RF coil (and therefore limited air circulation) and coils on the front-end of the acrylic mask where heat accumulation was expected first based on the warm air's tendency to rise. One temperature probe was placed inside the former to a center face position to quantify the effects of heat transfer through the former and to measure the temperature exposure of the subjects.

Magnetic Field Analysis and Assessment of Shim Results

The performance of the slice-specific DMC shim approach was compared in this study to zero through third order global static SH and slice-specific DSH shimming. To this end, the achievable magnetic field distributions after static SH, DSH and DMC shimming were derived theoretically and compared to experimental DMC shimming results. Static SH and DSH shimming was based on the 16 zero through third order SH functions. Theoretical DMC shimming utilized 48 MC basis fields that were calculated from the individual wire patterns of Fig. 1A by integration of the Biot-Savart law. Constrained least-squares fitting with the Levenberg-Marquardt method was applied to a single reference field map to decompose the magnetic field distribution over the whole brain for static SH shimming and

within axial brain slices for DSH and DMC shimming. An identical, slice-specific analysis with a set of calibrated MC basis fields was applied to derive the settings for experimental DMC shimming. Notably, all slice-specific shim settings were computed for the brain voxels of the considered slice plus the brain voxels from immediately neighboring slices. The magnetic field correction of the resultant thin 3-dimensional volumes accounted for potential through-slice magnetic field components and, thereby minimized intra-voxel phase spoiling and signal reduction [25].

The quality of the magnetic field homogeneity after theoretical or experimental shimming was assessed by the span of Larmor frequencies that included 50%, 80%, 85%, 90%, and 95% of the brain voxels and the standard deviation (S.D.) of the distribution of Larmor frequencies similar to [4; 25]. The use of the same reference field map together with the identical brain segmentations for the theoretical evaluation of the shimming methods guaranteed comparable results. The region-of-interest for the magnetic field analysis after experimental DMC shimming was based on the same reference brain segmentation, however, the signal-to-noise and the field error threshold criteria were reapplied to eliminate individual frequency outliers.

RESULTS

Quantification of Gradient-to-Multicoil and Multicoil-to-Multicoil Interactions

The peak voltages that were induced in open circuited MCs by 25 mT/m (or 50%) X, Y and Z test gradient switching in 512 µs did not exceed 2 V as determined by oscilloscope measurements. During operation of the constant-current amplifiers on the fully connected MC setup such gradient switching resulted in peak current alterations <2 mA. For a given MC, switching of 0.5 A test currents in neighboring MCs coil induced 125 µA peak responses, therefore the effects of all four MC neighbors led to a maximum current response of 0.5 mA. The observed gradient-to-MC and MC-to-MC effects were small compared to the applied MC current range of ± 1 A. Since the time constants of these effects were multiple times shorter than the repetition time delays between slice encoding steps, they were considered negligible for DMC shimming.

Impact of the Multi-Coil Setup on the RF Coil Performance

The impact of the MC setup on the RF coil performance was measured in phantoms (data not shown) and in human subjects (Fig. 2). To this end, multi-slice phase and B_1^+ maps were acquired for each of the 8 RF coil elements with and without the MC setup in place. The tuning and matching capability of the RF coil array was not affected by the MC device and its impact on the spatial phase distributions was limited. The presence of the MC setup did not significantly alter the shapes of the transmit B_1^+ fields, however, a uniform damping of 15–20% was observed for the B_1^+ amplitudes. The ability to obtain a homogeneous B_1^+ distribution was the same with the MC device inside the RF coil, albeit at a higher RF power requirement.

Demonstration of the Relative Magnetic Field Shaping Capabilities

Figure 3 shows a comparison of the magnetic field modeling characteristics of different shimming strategies (first row) and the corresponding outcome for magnetic field homogenization of the human brain at 7 Tesla (second row, except B). The magnetic field distribution of an example, centered axial slice (Fig. 3B) before shimming contained strong localized field artifacts mostly in the PFC (Fig. 3A). The zero through third order SH magnetic field analysis over the entire brain was necessarily a compromise for the shown slice and thus led to a relatively poor approximation of the present magnetic field distribution (Fig. 3C). The corresponding static shim field was not able to address the

localized, high-amplitude field focus in the PFC (Fig. 3D). The better utilization of the low order SH terms with zero through third order DSH shimming allowed a closer representation of the magnetic field distortion (Fig. 3E). The artifact in PFC was expected to be strongly reduced with DSH shimming at the cost of the creation of lower amplitude, band-shaped field gradients over large part of the brain slice due the limitations of the field modeling approach. The DMC concept for magnetic field modeling did not only provide a strong and localized field focus in the PFC similar to the original artifact, but also resembled the magnetic field distribution in the rest of the slice more closely (Fig. 3G). Correspondingly, DMC shimming removed the largest part of the magnetic field inhomogeneity (Fig. 3H). The magnetic field distribution after experimental DMC shimming proved the theoretical prediction of the shim outcome with some minor deviations in the anterior part of the brain (Fig. 3I).

Comparison of Static SH, DSH and DMC Shimming of the Human Brain at 7 Tesla

The computational extraction of the six human brains revealed target volumes for shimming of 46996 ± 4233 voxels corresponding to 1269 ± 114 mL (mean $\pm$ S.D.). Before shimming, the frequency spans covering 50%, 80%, 85%, 90% and 95% of the brain voxels were determined to 120 ± 35 Hz, 262 ± 68 Hz, 308 ± 76 Hz, 375 ± 91 Hz and 455 ± 91 Hz (mean $\pm$ S.D.), respectively, and the standard deviation of the brains' frequency distribution was measured to 113 ± 18 Hz (mean $\pm$ S.D.).

Theoretical shimming with static zero through third order SH terms reduced the frequency measures to 24–184 Hz and the S.D. to 43 Hz (Table 1, column 2) and theoretical DSH shimming allowed further improvements to 16–113 Hz and 30 Hz (Table 1, column 3), respectively. Theoretical DMC shimming resulted in the most homogeneous magnetic field distributions over the six brains with frequency spans of 10–80 Hz and a S.D. of 23 Hz (Table 1, column 4). The frequency measures after experimental DMC shimming of 13–94 Hz and the S.D. of 25 Hz were better than after static SH or DSH shimming, however, the theoretical predictions were not fully reached (Table 1, column 5).

The magnetic field components in peripheral, ventral and dorsal axial brain slices before shimming were typically simple in nature (Fig. 4, first row) and could be adequately addressed by static zero through third order SH shimming (Fig. 4, second row). However, whole brain SH shimming was not able to account for any localized features and the strong distortions in the central part of the brain were hardly affected. Notably, residual magnetic field imperfections were observed in the peripheral brain slices in some cases depending on the overall brain geometry, the details of the major field artifacts and the applied brain segmentation. The magnetic field artifacts in the central slices covering the PFC and the TLs could be more efficiently minimized with DSH shimming (Fig. 4, third row) in slices with peripheral field artifacts such as in the lower TLs in slice 3 in which the artifact was mostly limited to the anterior part of the brain. In slices with confined and localized foci (e.g. slices 4–6), the complexity of the necessary shim fields exceeded the modeling capability of DSH shimming and the inhomogeneities could only be compensated partially. In fact, the reduction of the major, high amplitude field artifacts with DSH shimming was achieved at the cost of inducing some lower amplitude magnetic field alterations in other parts of the brain by the shimming process. Theoretical DMC field modeling based on Biot-Savart simulations allowed the synthesis of magnetic shim fields that included complex, localized features to address the artifacts in the PFC and the TLs and shallow components for the compensation of the large-scale artifact terms that were apparent throughout the brain (Fig. 4, fourth row). The negative field foci in slice 3 were too localized to be synthesized by any of the considered shimming methods, thereby leading to similar resultant field artifacts (blue spots). Magnetic field distributions after experimental DMC shimming were generally consistent with their theoretical predictions (Fig. 4, fifth row) and the resultant whole brain

magnetic field homogeneity exceeded the outcome of zero through third order DSH shimming (Table 1). However, some residual imperfections remained (e.g. in slices 3 and 4) with this first implementation. Note that the experimental magnetic field maps were acquired after a single adjustment and no further corrections have been applied.

Figure 5 summarizes the shim performances of theoretical static SH, DSH and DMC as well as experimental DMC shimming for selected central slices of all six subjects of this study (Fig. 4, first to fourth row, respectively). Severe localized magnetic field artifacts remained after static SH shimming in the PFC and the TLs that could be strongly reduced with DSH shimming at the cost of introducing broad low-amplitude gradient bands over large parts of the slices. A limited range of magnetic field amplitudes has been chosen in this figure to focus on the details of the DSH and DMC shimming. The residual magnetic field artifacts after static SH shimming largely exceeded these boundaries due to the limited performance of the method. Note the difference between magnetic field foci that are a direct consequence of anatomy-based and susceptibility-induced field alterations (e.g. in the PFC and the TLs) and those generated as secondary effects by inadequate shim fields. The superior magnetic field modeling capacity of the DMC approach manifested itself not only in the reduction of the primary field foci in the PFC and the TLs, but moreover in the avoidance of secondary magnetic field alterations in the other parts of the brain. Experimental DMC shimming could be successfully applied in all six subjects of the study, thereby validating the DMC shim concept, however, some variation between theoretical predictions and experimental results of DMC shimming remained.

DISCUSSION

Methodological and Technical Considerations

The manuscript introduces DMC shimming of the human brain at 7 Tesla with a set of individual, circular coils. The MC basis fields were generated by 48 simple coils driven in the ±1 A range and were neither specifically tailored to the magnetic field distortions like in [3] nor were they required to be orthogonal as in [29]. However, together they provided a repertoire of field shapes that included strong local gradient patterns close to the individual coils and shallow field shapes farther away from them. The combination of these basis fields has been shown theoretically and experimentally in this study to provide unprecedented levels of magnetic field homogeneity in the human brain at 7 Tesla. Some differences between the theoretical predictions and experimental results remained, however, and the presented first implementation of the MC concept in the human brain has not yet reached the accuracy level of earlier MC installations in miniaturized setups [24; 25]. The reproducible positioning of the MC setup inside the MR scanner is considered key for an accurate synthesis of MC shim fields. This study consisted of six DMC shimming experiments from 3 sessions that were spread over 2 months and were based on calibrated MC basis fields from a fourth, earlier session. In the previous implementations, solid MC setups were mounted immediately to the scanner bore to guarantee a high degree of mechanical stability and position reproducibility. In this study, the limited available space between the RF coil and the subject heads did not allow an equally solid mounting. In fact, the combined RF and MC setup could not be mounted directly to the scanner, but had to be attached to the patient bed. Depending on the subjects' weight and body mass distribution, variable deflection of the bed was observed due to its canter-levered nature. Point-like positioning probes were therefore integrated into the MC former, their positions were determined with MR images for each subject and a position adjustment of the scanner bed was applied to correct for the translational shifts of the MC setup (with an accuracy of 1–2 mm). The rotational component introduced by the bed flexing around the scanners' X (i.e. left-to-right) axis was <0.5 degrees in all cases and has been neglected so far. The accurate measurement of the translational and rotational components of the MC setup with a FASTMAP-like approach

[4; 16] along the generated MC basis fields and the subsequent incorporation of this information into the MC basis set is expected to eliminate the time-consuming and error prone adjustments during the experiment preparation and to improve future DMC shimming. Notably, the quality of the applied MC currents was not considered a significant error source for the generation of DMC shimming in this study due to a current resolution of 122 µA and a current stability <50 ppm of the home-built amplifier system [25].

The RF coil was considered a given in this study and the MC setup was engineered to fit between the subject head and the former of the RF coil array. The lack of physical proximity of the MC setup and the RF array inherently minimized unwanted interactions between the two coil systems (Fig. 2) and allowed their simultaneous usage. The explicit, closer integration of RF antennas and MC matrix shimming into a single setup in future designs bears considerable potential for a further optimization of the DMC magnetic field modeling capability, improved RF performance and the minimization of the overall space requirement of both systems. Such optimization will greatly benefit from electromagnetic field calculations for the quantitative assessment of MC-to-RF interactions and their impact on the RF performance, which has not been done here and has to be the subject of future research. The equitable design of an integrated RF/MC system will also allow a mechanical reinforcement of the former hosting t he MC coils (e.g. with epoxy), thereby further reducing the variance of the DMC magnetic field synthesis.

The full dynamic ±1 A range of the 48 current amplifiers was regularly applied for DMC shimming in this study. The applied coil current for DMC shimming averaged over all brains and all slices was 304 mA corresponding to 0.6 W per coil or 29 W for the entire MC setup. The maximum time-averaged power deposition within an individual coil in this study was measured to 1.3 W (662 mA). Notably, the coil with the maximum current requirement and the maximum concomitant heat deposition differed between subjects. Temperature changes of the MC coils remained below 5 degrees Celsius over the course of the 10 minutes DMC shimming experiments at all times (data not shown) and active cooling of the MC system was not necessary. In the presented implementation, the DMC shim field for a specific slice was applied immediately after completion of the signal readout of the previous slice, i.e. DMC shim fields were applied continuously. Further reductions of the duty cycle and the concomitant coil heating are possible at no penalty by a temporary disabling of the DMC fields after readout completion with a delayed application of the next DMC shim field closer to the onset of the consecutive slice-selective MR sequence step for which it is intended.

No significant coil-to-coil interactions were observed as a result of the fast MC field switching and the complete absence of eddy currents with DMC shimming is considered an advantage over DSH shimming when accomplished with the scanners' SH shim coils for which the proximity to the cold conducting structures in the scanner bore typically leads to a multitude of artifacts. Their measurement and compensation is cumbersome, but essential for the successful implementation of DSH shimming [4]. A down-scaling of the SH coil system from the size of the scanner bore e.g. to the size of the applied DMC setup would prevent the generation of eddy currents and lead to efficiency gains of the SH field generation. However, given that the SH shims are typically not current (i.e. amplitude) limited, the shimming performance would not improve as the shim field shapes are described by functions that are independent of physical shim coil size.

Assessment of Shim Performance

The performance comparison of different magnetic field modeling techniques for shimming the human brain at 7 Tesla was achieved based on quality measures for magnetic field homogeneity, namely the span of Larmor frequencies to include 50% to 95% of the brain

voxels and the standard deviation of the frequency distribution over the brain. The inclusion of the cerebellum was used as whole brain segmentation criterion together with user-independent reliability measures for the magnetic field quantification within brain voxels. The reduction or extension of this whole brain definition will (similar to the concept of dynamic shimming) alter the performance of static SH shimming, but the dynamic shimming methods, i.e. DSH and DMC shimming, will remain unaffected (expect for the effect of the extension or reduction on the whole brain homogeneity measure). The theoretical comparisons of the shimming methods was based on identical magnetic field mapping data along with the same regions-of-interest and, therefore the analysis results are inherently comparable. The numerical values for the frequency span measures in that analysis remained largely unaffected by the details of the brain segmentation due to their focus on the bulk voxels and the relative expression of the shim performances e.g. for DMC shimming with respect to DSH shimming proved particularly immune. The standard deviation (S.D.) was more susceptible to the inclusion or exclusion of individual frequency outliers and, therefore more prone to the details of the brain segmentation. The magnetic field analysis itself, i.e. the decomposition of the reference field map into the various basis field sets, was not affected by minute details of the brain extraction due to the negligible statistical power of individual frequency outliers.

Comparison of Shim Approaches

DMC shimming was compared in this study to zero through third order DSH shimming which is the current state-of-the-art shimming method for the entire human brain [4]. The consideration of theoretical DSH shimming furthermore corresponds to an ideal implementation of such system and, therefore, must be labeled the gold standard for human brain shimming so far. Theoretical and experimental DMC shimming have been demonstrated in this study to be better suited for the compensation of the complex magnetic field distortions encountered in the human brain at 7 Tesla than SH-based shimming, including zero through third order DSH shimming. It has been shown previously that static global shimming of the human brain with zero to third, fourth or fifth order SH terms cannot compete with zero to third order DSH shimming [4]. DMC shimming of the six subject brains considered in this study furthermore reveals frequency span measures with average reductions of 50%, 42% and 36% compared to static (unconstrained) fourth, fifth and even sixth order theoretical SH shimming, respectively. Similarly, DMC shimming allowed 35% reduced frequency span measures compared to zero through third order DSH shimming (Table 1) and even full fourth order DSH shimming is outperformed by 16%. Static whole brain shimming with the MC approach has been demonstrated in the mouse brain before [25] and simulations for the presented setup predict a 2% average deviation of the quality measures compared to zero through third order DSH shimming, corresponding to a similar performance of both methods. Note that the MC setup in this study was by no means optimized for static MC shimming, as it was solely designed for DMC shimming and no efforts were made to account for potential static applications.

Realistic constraints for DSH shimming were used for the comparison of shimming methods in this study based on the institutes' gradient and shim system [4], however, only 1.8% of the DSH settings were amplitude limited with the imposed constraints of which the Z2 SH term accounted for 55%. Due to the small number of constrained terms and their minor effective limitation, the frequency measures were not significantly improved by an open, unconstrained analysis. In other words, the considered set of SH shim amplitudes has been proven sufficient for successful zero through third order DSH shimming of the human brain at 7 Tesla and the available magnetic field homogeneity was limited by the inadequacy of the SH shape repertoire rather than by the available amplitude range. The limited magnetic field modeling capacity of DSH shimming manifested itself not only in incomplete removal

of the strong and localized field foci encountered in the PFC and the TLs, but also in magnetic field alterations in other parts of the brain concomitant to DSH shimming. Trade-offs between major focus depths and the general homogeneity over the (rest of the) brain can be achieved e.g. through amplitude weighting of the cost function in the shim algorithm [4], however, true homogeneity improvements cannot be realized with such approach.

The basic patterns of the major, susceptibility-induced field distortions were found to be similar in all subjects, but considerable inter-subject variability was observed for the details of their absolute and relative position, spatial extension and depth (Fig. 5). A successful shim method furthermore must tolerate the inevitable uncertainties in subject placement. Magnetic field modeling with the DMC approach has been shown in this study to closely resemble the magnetic field distributions encountered in the human brain at 7 Tesla across subjects. Correspondingly, DMC shimming reduced the magnetic field foci in the PFC and the TLs while avoiding significant field alterations in other parts of the brain concomitant to static SH and DSH shimming.

The larger number of 48 basis field shapes for DMC shimming led to an increased effort for the experimental calibration of the MC shim system when compared e.g. to the 15 terms of zero through third order DSH shimming. However, this calibration has to be done only once and can be fully automated. The increased computational burden of the field optimization for DMC compared to DSH shimming due to the larger parameter space is typically <15 s for all 40 slices and can be considered negligible compared to the time requirements of other components of the shimming process, i.e. magnetic field mapping, data handling, further processing steps and upload of the shim settings to the amplifier hardware. Neither the calibration of the MC setup nor the DMC shimming process itself are conceptually more complex than with SH-based methods.

Potential of Dynamic Multi-Coil Shimming

MR imaging, spectroscopy and spectroscopic imaging sequences are typically set up as multi-slice or multi-voxel acquisitions and the application of DMC shimming is possible at no penalty. Furthermore, DMC shimming is by no means limited to this specific slice orientation and dedicated shim fields can be generated for any other slice orientation or over 3-dimensional volumes such as cubic or anatomy-based shapes (data not shown). Functional MR imaging based on gradient echo methods is particularly sensitive to magnetic field inaccuracies [2]. The homogeneity improvements that can be realized with DMC shimming are expected to directly translate into improvements of the data quality for functional MR imaging of the human brain at 7 Tesla similar to the improvements that were achieved on mouse brain [25]. Alterations to the MC positions can be applied to allow the integration of specific stimulation equipment for functional MR studies. The MC approach does not critically rely on the exact details of the coil matrix and other MC geometries are also possible including its placement on the outside of the RF coil [25]. In fact, the flexibility of the MC positioning has been applied in this study by leaving a central 10 cm band around the subject heads uncovered to minimize interactions with the RF coil array. DMC shimming has been shown to be scalable from a miniaturized setup for the mouse brain [25] to applications in the human brain. There is no obvious reason, why a further expansion of the presented head-sized DMC system to a size that allows whole body shimming should not be possible. Furthermore, the flexibility in the design of the MC matrix makes DMC shimming a prime candidate for localized applications in spine, breast, prostate or the extremities. The presented setup can be adopted to even higher scanner B_0 field strengths through an increase of the number of turns per coil or an increase of the available current range. Increased magnetic field modeling capabilities are expected from further improvements of the MC matrix. In particular, an expansion of the coil array combined with a miniaturization of the individual coils will improve the complexity of magnetic field

patterns that can be generated. The magnetic fields after DMC shimming with a 48 coils setup were shown to be largely flat and the achieved magnetic field homogeneity is adequate for most MR applications. Future DMC developments might therefore also be dedicated towards an integrated magnetic field modeling system capable of generating all fields necessary to perform MR experiments in the human brain including spatial selection [30], spatial encoding and shimming.

A novel shimming technique for the human brain has been introduced that is based on the combination of generic, non-SH field shapes generated by simple circular coils. The MC field modeling approach enabled the flexible generation of complex magnetic field shapes and DMC shimming was shown to allow considerably improved magnetic field homogenization over the human brain at 7 Tesla compared to zero through third order DSH shimming. The presented MC shimming technique paves the way for high field MR applications of the human brain for which excellent magnetic field homogeneity is a prerequisite.

Supplementary Material

Refer to Web version on PubMed Central for supplementary material.

Acknowledgments

References

1. de Graaf, RA. In Vivo NMR Spectroscopy: Principles and Techniques. London: John Wiley and Sons; 2008. p. 484-502.

2. Jezzard P, Clare S. Sources of distortion in functional MRI data. Hum Brain Mapp. 1999; 8:80–85. [PubMed: 10524596]

3. Juchem C, Nixon TW, McIntyre S, Rothman DL, de Graaf RA. Magnetic field homogenization of the human prefrontal cortex with a set of localized electrical coils. Magn Reson Med. 2010; 63:171–180. [PubMed: 19918909]

4. Juchem C, Nixon TW, Diduch P, Rothman DL, Starewicz P, de Graaf RA. Dynamic Shimming of the Human Brain at 7 Tesla. Concepts in Magnetic Resonance. 2010; 37B:116–128. [PubMed: 20657809]

5. Ugurbil K, Adriany G, Andersen P, Chen W, Garwood M, Gruetter R, Henry PG, Kim SG, Lieu H, Tkac I, Vaughan T, Van De Moortele PF, Yacoub E, Zhu XH. Ultrahigh field magnetic resonance imaging and spectroscopy. Magn Reson Imaging. 2003; 21:1263–1281. [PubMed: 14725934]

6. Levy R, Goldman-Rakic PS. Segregation of working memory functions within the dorsolateral prefrontal cortex. Exp Brain Res. 2000; 133:23–32. [PubMed: 10933207]

7. Miller EK, Freedman DJ, Wallis JD. The prefrontal cortex: categories, concepts and cognition. Philos Trans R Soc Lond B Biol Sci. 2002; 357:1123–1136. [PubMed: 12217179]

8. Hains AB, Arnsten AF. Molecular mechanisms of stress-induced prefrontal cortical impairment: implications for mental illness. Learn Mem. 2008; 15:551–564. [PubMed: 18685145]

9. Sigala N, Logothetis NK. Visual categorization shapes feature selectivity in the primate temporal cortex. Nature. 2002; 415:318–320. [PubMed: 11797008]

10. Van Paesschen W. Qualitative and quantitative imaging of the hippocampus in mesial temporal lobe epilepsy with hippocampal sclerosis. Neuroimaging Clin N Am. 2004; 14:373–400. vii. [PubMed: 15324854]

11. van den Heuvel MP, Hulshoff Pol HE. Exploring the brain network: a review on resting-state fMRI functional connectivity. Eur Neuropsychopharmacol. 2010; 20:519–534. [PubMed: 20471808]

12. Robinson RJ, Bhuta S. Susceptibility-Weighted Imaging of the Brain: Current Utility and Potential Applications. J Neuroimaging. 2011

13. Speck O, Stadler J, Zaitsev M. High resolution single-shot EPI at 7T. Magma. 2008; 21:73–86. [PubMed: 17973132]

14. Shen J, Rothman DL, Hetherington HP, Pan JW. Linear projection method for automatic slice shimming. Magn Reson Med. 1999; 42:1082–1088. [PubMed: 10571929]

15. Chen Z, Li SS, Yang J, Letizia D, Shen J. Measurement and automatic correction of high-order B0 inhomogeneity in the rat brain at 11.7 Tesla. Magn Reson Imaging. 2004; 22:835–842. [PubMed: 15234452]

16. Gruetter R. Automatic, localized in vivo adjustment of all first- and second-order shim coils. Magn Reson Med. 1993; 29:804–811. [PubMed: 8350724]

17. Morrell G, Spielman D. Dynamic shimming for multi-slice magnetic resonance imaging. Magn Reson Med. 1997; 38:477–483. [PubMed: 9339449]

18. Blamire AM, Rothman DL, Nixon T. Dynamic shim updating: a new approach towards optimized whole brain shimming. Magn Reson Med. 1996; 36:159–165. [PubMed: 8795035]

19. de Graaf RA, Brown PB, McIntyre S, Rothman DL, Nixon TW. Dynamic shim updating (DSU) for multislice signal acquisition. Magn Reson Med. 2003; 49:409–416. [PubMed: 12594742]

20. Koch KM, McIntyre S, Nixon TW, Rothman DL, de Graaf RA. Dynamic shim updating on the human brain. J Magn Reson. 2006; 180:286–296. [PubMed: 16574443]

21. Wilson JL, Jenkinson M, Jezzard P. Optimization of static field homogeneity in human brain using diamagnetic passive shims. Magn Reson Med. 2002; 48:906–914. [PubMed: 12418007]

22. Cusack R, Russell B, Cox SM, De Panfilis C, Schwarzbauer C, Ansorge R. An evaluation of the use of passive shimming to improve frontal sensitivity in fMRI. Neuroimage. 2005; 24:82–91. [PubMed: 15588599]

23. Hsu JJ, Glover GH. Mitigation of susceptibility-induced signal loss in neuroimaging using localized shim coils. Magn Reson Med. 2005; 53:243–248. [PubMed: 15678531]

24. Juchem C, Nixon TW, McIntyre S, Rothman DL, de Graaf RA. Magnetic field modeling with a set of individual localized coils. J Magn Reson. 2010; 204:281–289. [PubMed: 20347360]

25. Juchem C, Brown PB, Nixon TW, McIntyre S, Rothman DL, de Graaf RA. Multi-Coil Shimming of the Mouse Brain. Magn Reson Med. 2011 *in press*.

26. Avdievich NI, Pan JW, Baehring JM, Spencer DD, Hetherington HP. Short echo spectroscopic imaging of the human brain at 7T using transceiver arrays. Magn Reson Med. 2009; 62:17–25. [PubMed: 19365851]

27. Sacolick LI, Wiesinger F, Hancu I, Vogel MW. B1 mapping by Bloch-Siegert shift. Magn Reson Med. 2010; 63:1315–1322. [PubMed: 20432302]

28. Nixon, TW.; Juchem, C.; McIntyre, S.; Rothman, DL.; de Graaf, RA. Design and Implementation of a Real Time Multi-Coil Amplifier System, ISMRM, annual meeting; Stockholm, Sweden. 2010. p. 1532

29. Romeo F, Hoult DI. Magnet field profiling: analysis and correcting coil design. Magn Reson Med. 1984; 1:44–65. [PubMed: 6571436]

30. Juchem, C.; Nixon, TW.; Brown, PB.; McIntyre, S.; Rothman, DL.; de Graaf, RA. Spatial Selection Through Multi-Coil Magnetic Field Shaping, ISMRM, annual meeting; Montreal, Canada. 2011. p. 385
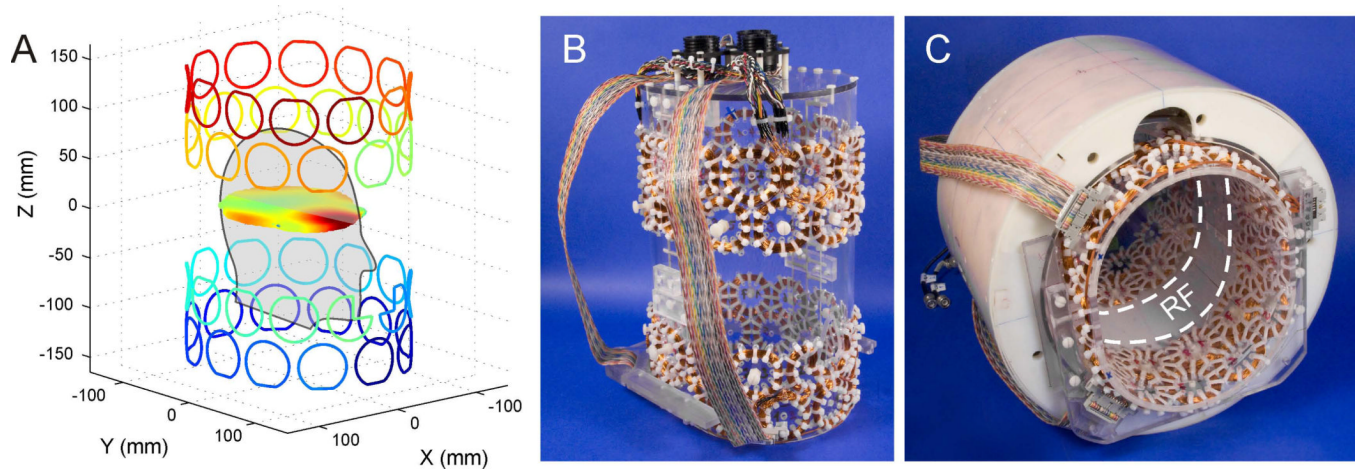
Fig. 1. DESIGN AND IMPLEMENTATION OF THE MULTI-COIL SETUP
Theoretical design and experimental implementation of the 48-channel multi-coil setup for magnetic field homogenization of the human brain at 7 Tesla. (A) Magnetic field modeling for dynamic MC shimming in axial slices was achieved through superposition of 48 basis field shapes that were generated by a matrix of 48 independently driven (as indicated by the varying color coding), circular coils. (B) In its experimental realization, the coil matrix consisting of 4 rows of 12 coils (100 turns, center diameter 47 mm) was mounted on the surface of an acrylic structure together with probes for temperature monitoring (not visible). (C) The close integration of the MC setup with the available RF coil array allowed their simultaneous use. Interactions of the MC setup with the centered, single ring of 8 RF coil elements were minimized by design through avoidance of physical overlap of both systems.
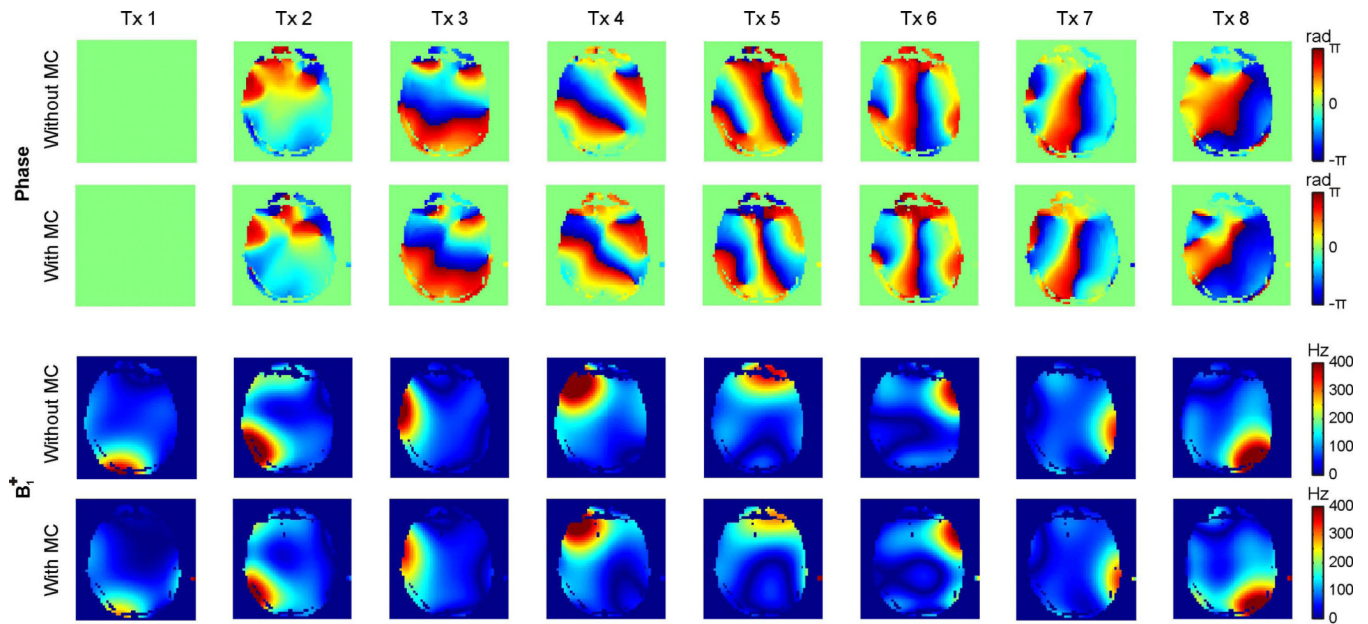
Fig. 2. IMPACT OF MULTI-COIL SETUP ON RADIO-FREQUENCY BEHAVIOR
Impact of the DMC shimming device on the 8-channel Tx/Rx RF performance. Phase maps remained largely unaffected by the presence of the MC setup inside the RF coil, while a homogeneous B_1^+ damping of 15–20% was observed. The B_1^+-shimming capability was not affected by the presence of the MC device.
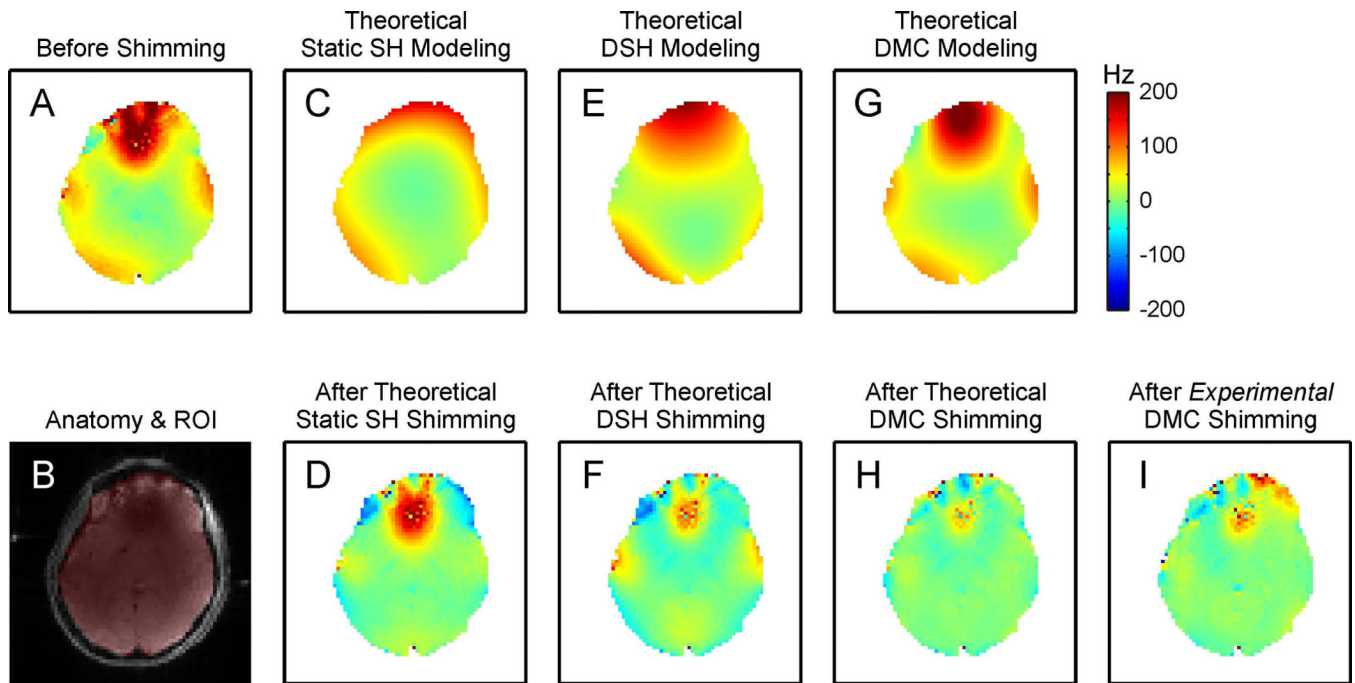
Fig. 3. DETAILED COMPARISON OF SHIMMING METHODS
Magnetic field modeling characteristics of different shimming strategies (first row) and their performance for shimming the human brain at 7 Tesla (second row, except B). The zero through third order SH functions allowed the synthesis and removal of shallow magnetic field components, but significant imperfections remained throughout the brain or were even induced (C–F). The DMC approach was capable of generating a magnetic field distribution that more closely resembled the original distortion over the entire slice including the strong and localized field focus in the PFC (G). Correspondingly, DMC shimming removed the largest part of the magnetic field inhomogeneity as predicted theoretically (H) and shown experimentally (I). (See text for details)
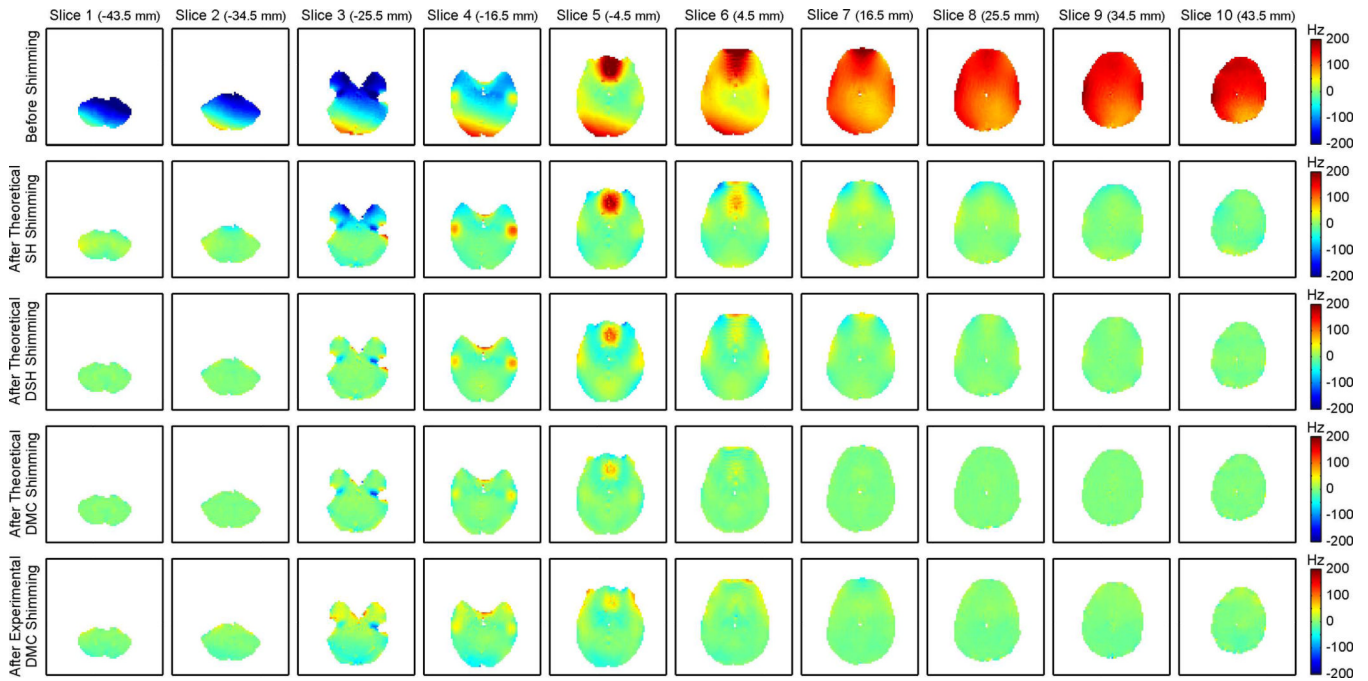
Fig. 4. MUTLI-SLICE COMPARISON OF SHIMMING METHODS
Comparison of zero through third order static SH, DSH and DMC shimming for axial multi-slice shimming of the human brain at 7 Tesla. Before shimming, a combination of shallow, large-scale field components and localized, high-amplitude field foci was observed (first row). Static SH shimming was capable of removing the shallow terms (second row) and DSH shimming furthermore minimized some of the localized components (third row). Theoretical DMC shimming (fourth row) performed equally well in slices with shallow components only (dorsal and ventral slices) and outperformed DSH shimming in slices that contained more complex field artifacts (center slices). Experimentally measured magnetic field distributions in the presence of DMC shimming (fifth row) proved the theoretical concept and outperformed DSH shimming (compare Table 1).
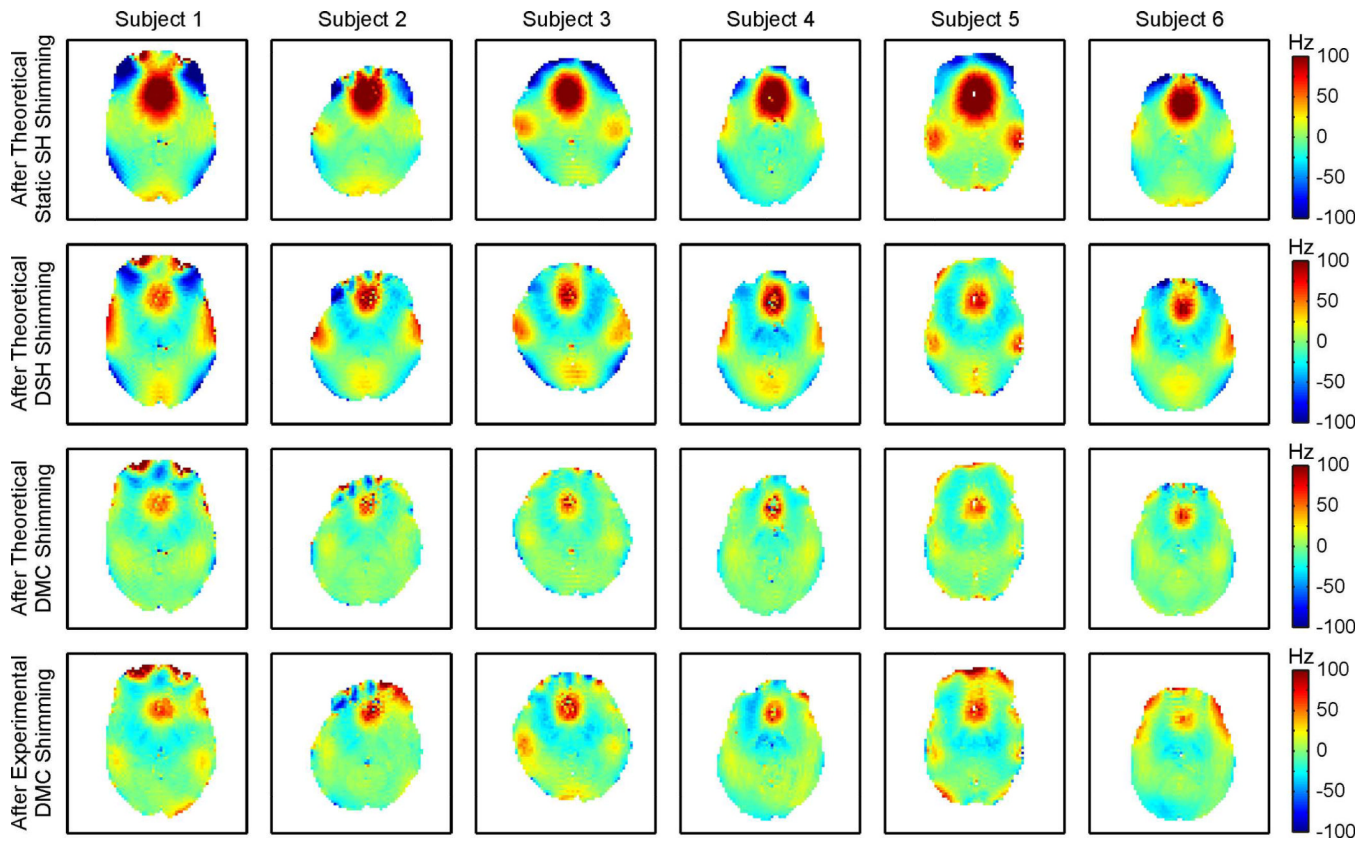
Fig. 5. COMPARISON OF SHIMMING METHODS OVER ALL SUBJECTS
Performances of zero through third order static SH, DSH and DMC shimming of the human brain at 7 Tesla across all 6 subjects of the study. The residual magnetic field imperfections after theoretical SH shimming (first row) and after DSH shimming (second row) were further reduced with the DMC shim approach (third row). Experimental DMC shimming was successful in all subjects and outperformed DSH shimming, however, the full potential of DMC shimming of the human brain has not yet been realized with this first realization (fourth row, compare Table 1).

Table 1

Theoretical predictions and experimental results of zero through third order static SH shimming, dynamic SH shimming and dynamic MC shimming of the human brain at 7 Telsa across the 6 subjects of the study given as standard deviation (S.D.) and 50%..95% frequency span measures (all values in Hertz, mean ± S.D.).

Measure	Static SH Shim Theory	Dynamic SH Shim Theory	Dynamic Multi-Coil Shim Theory	Dynamic Multi-Coil Shim Experiment
50%	24 ± 5	16 ± 3	10 ± 2	13 ± 1
80%	67 ± 17	48 ± 13	29 ± 8	37 ± 8
85%	87 ± 21	59 ± 15	38 ± 11	47 ± 9
90%	121 ± 30	78 ± 19	51 ± 15	62 ± 14
95%	184 ± 50	113 ± 27	80 ± 25	94 ± 20
S.D.	43 ± 10	30 ± 7	23 ± 7	25 ± 6